

## NOVEL ABSORBERS BASED ON WIDEBAND ANTENNA ARRAY FOR RCS REDUCTION

Fang-Yao Kuo, Pai-Shiuan Wang, Cheng-Yuan Chin, and Ruey-Bing Hwang\*

Department of Electrical Engineering, National Chiao Tung University, 1001, Ta-Hsueh Road, Hsinchu 300, Taiwan

**Abstract**—This study presents a novel wideband absorber for radar cross section (RCS) reduction. Unlike previous absorber designs that use multilayer lossy materials, this study proposes a design based on a planar antenna array that adopts a bowtie dipole structure as the unit cell. The complete design procedure was investigated by using examples for single- and dual-polarized incident wave designs. The measurement results show that the bandwidth of both designs exceeded 81% of 10 dB RCS reduction when the thickness is less than 12% of the free space wavelength at the lowest operating frequency. The high RCS reduction of the proposed absorbers was demonstrated using commercial ground-penetrating radar. Results show that the proposed absorber is invisible to radar.

### 1. INTRODUCTION

Researchers have previously studied a wide variety of designs for electromagnetic wave absorption to meet the demands of both military and civil applications. The main focus of civil applications is to reduce the electromagnetic interference among microwave components and electronic circuits at a certain narrow band. Unlike the radar absorbing material (RAM) designs for civil applications, RAM designs for military applications must fulfill several unique requirements, such as a wide bandwidth, a thin thickness, and a low profile. First, because a radar system sends out short pulse signals in the time domain for object detection, RAM with a wide bandwidth can help reduce the echoes of the pulses that scatter off the target and return to the radar.

---

*Received 18 March 2013, Accepted 31 May 2013, Scheduled 6 June 2013*

\* Corresponding author: Ruey-Bing Hwang (raybeam@mail.nctu.edu.tw).

Second, a compact, thin, surface-coated RAM is desirable to maintain the high maneuverability of military vehicles and meet aerodynamics requirements.

Researchers have developed two main RAM designs. The first approach is to redirect the impinging wave away from the incident direction, producing significant backward RCS reduction [1–4]. Paquay et al. [1] presented a design based on a combination of artificial magnetic conductor (AMC) cells and perfect electric conductor (PEC) cells in a chessboard-like configuration. The waves reflected from the AMC and PEC have opposite phases near the resonant frequency of the AMC. The reflection from an incident plane wave normally impinging on the chessboard structure can be cancelled out by using the approximation of the antenna array factor. However, because the zero reflection phase of an AMC covers a relatively narrow frequency band, it cannot provide a wide operation band. To enhance the bandwidth effectively, other approaches replace the combination of PEC and AMC with a composite AMC structure [2–4] that consists of two types of AMCs with different reflection phase characteristics.

The other approach is to absorb the incoming wave. Dallenbach layers [5] and Salisbury screens [6] represent two of the oldest and simplest types of absorbers. The Dallenbach layer consists of a homogeneous lossy material that can dissipate the energy of an incident wave. With the right relative permittivity and permeability, this material can be impedance-matched to free space, minimizing reflection at the air-material interface. Unfortunately, it is difficult to find materials with the appropriate dielectric and magnetic properties to act as a matched RAM over a certain frequency range. Therefore, Landy et al. [7] introduced metamaterials to create a thin absorber in the microwave band in 2008. Although metamaterials typically exhibit high losses around the resonance frequency and limit the practical applications requiring high efficiencies, losses can facilitate the absorption of incoming electromagnetic power. To meet the stringent requirements imposed by absorber applications, several efforts have been devoted to achieving an enhanced bandwidth [8, 9], a wide incident angle [10–15], and polarization-insensitive absorption [8, 11, 13–15]. Despite the advantages of metamaterial absorbers, they suffer from the inherent drawback of a narrow bandwidth.

The Salisbury screen is another simple resonant absorber that consists of a thin resistive sheet located a quarter-wavelength above a conducting plate. This type of absorber exhibits a narrow operating frequency band and occupies a thick space for transforming the impedance of the conducting plate to an open circuit. A new metallic

electromagnetic structure, which possesses the characteristic of a high impedance surface (HIS) near the resonance frequency, has been recently investigated to replace the PEC ground plane for reducing the thickness of Salisbury screens [16–18]. A surface with a high surface-impedance boundary condition, which is defined as the ratio between the tangential electric and magnetic fields on the surface, can mimic the reflection characteristics of a perfect magnetic conductor (PMC). In this case, the long impedance-transformed path from the ground plane to the resistive sheet is unnecessary. Because the Salisbury screen has a resistor-loaded HIS, it exhibits a broad bandwidth and a wide incident angle. Lossy metallic frequency selective surfaces (FSSs) [19–21], placed above a thin grounded dielectric substrate, can replace the ohmic loss of a resistive sheet to reduce the thickness of the Salisbury screens. However, the design and fabrication of lossy FSSs are complex and uneconomical.

This paper presents the novel design of an antenna-based absorber for the RCS reduction with single/dual polarization in the microwave band. Based on the desirable features of a wide operation band and a simple design of a bowtie-shaped antenna, the proposed design adopts a bowtie dipole with a lumped resistor as the unit cell of a two-dimensional periodic array. This bow-tie structure receives incoming electromagnetic waves at normal incidence and then dissipates these waves by the resistive load in the operating bandwidth, decreasing the scattered energy from the structure. To improve the single polarization characteristics of a bowtie antenna, a cross bowtie structure is adopted to implement a dual-polarized absorber. Measurement results show that the bandwidths of both designs are over 81% of 10 dB RCS reduction when the thickness is less than 12% of the free space wavelength at the lowest operating frequency. An experiment involving a commercial ground-penetrating radar shows the high RCS reduction of the proposed absorber.

## 2. UNIT CELL DESIGN AND CONFIGURATION

Antennas are generally designed to transform free space impedance to real impedance in either 50 ohm or 75 ohm systems and to transmit the received signal to a back-end system. In this study, the design of an absorber is similar to that of an antenna, but the absorber is terminated by a resistive load to dissipate the incoming wave. Figure 1 shows the configuration and definition of parameters for one unit cell of the proposed periodic resistive arrays, where (a) Unit Cell I and (b) Unit Cell II are the designs for single- and dual-polarization, respectively. Because the bowtie dipole possesses a wide operating band and good

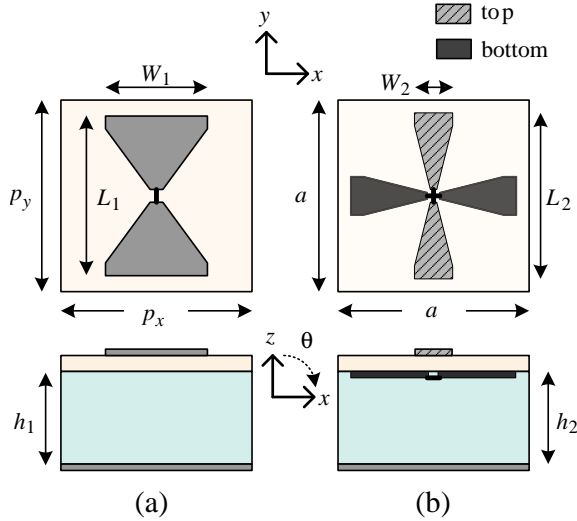


**Figure 1.** Configurations and definitions of parameters for one unit cell of the proposed periodic resistive array, where (a) Unit Cell I and (b) Unit Cell II are the designs for single- and dual-polarization, respectively.

efficiency in the antenna case, it is a good candidate for matching between the free space and the resistive load in a wide frequency band. This bowtie structure, when printed on a dielectric substrate, is separated from the conducting plate by an air space. In circuitry terminology, the air space is equivalent to a transmission line that transfers the impedance from the short-circuited conducting plate to the bowtie. Therefore the absorber can achieve a wideband response with the proper adjustment of the air space thickness. The thickness of the air space also affects the operating frequency of the absorber because of the coupling of the bowtie dipole image caused by the ground plane. The chip resistor is inserted in the center of the bowtie to absorb incoming waves. The resistive load terminates and consumes the surface current on the bowtie structure, induced by the incident plane wave. In the dual-polarization design, the cross bowtie dipoles shown in Figure 1(b) are orthogonal to each other to minimize the coupling. The dipoles have the same dimensions and are arranged in a parallel plane separated by a substrate to reduce the backward RCS when it is normally incident by either a vertical- or horizontal-polarization plane wave.

### 3. SIMULATION AND ANALYSIS

The proposed bowtie structure is designed on a 0.8 mm FR-4 epoxy substrate with a relative dielectric constant  $\epsilon_r = 4.3$  and a loss tangent  $\tan \delta = 0.02$ . Unit cell analysis and optimization were performed using Computer Simulation Technology (CST) Microwave Studio [22]. Both single- and dual-polarized designs were fabricated based on the optimum combinations of the parameters listed in Table 1. Figure 2 shows the unit cell model of Unit Cell I as simulated in CST MWS, where a resistive load at the center serves as the terminator. Unit cell boundary conditions (UCBCs) are applied in both the  $x$ - and  $y$ -directions, and Floquet port excitations as plane waves are set up in the positive  $z$ -direction. Figure 3 shows the predicted frequency response of Unit Cell I based on the Floquet theory and the simulation result of an ideal Salisbury screen for comparison. The resonance frequency of the conventional Salisbury screen absorber is 5 GHz, and the distance between the thin resistive sheet and conducting plate is 15 mm. The  $-10$  dB reflection coefficient bandwidth of the proposed

**Table 1.** Optimum combinations of physical parameters for single- and dual-polarization.

$L_1$	$W_1$	$h_1$	$p_x$	$p_y$	$R_1^*$	$L_2$	$W_2$	$h_2$	$a$	$R_2^*$
21	19	10	30	27	150	27	10	10	30	130
mm	mm	mm	mm	mm	$\Omega$	mm	mm	mm	mm	$\Omega$

(\*: resistance of the terminated load in Unit Cell I and Unit Cell II, respectively).

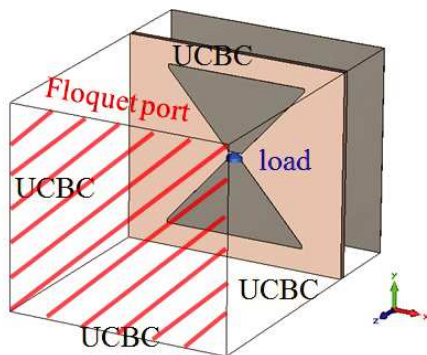


**Figure 2.** Unit cell model of Unit Cell I in Figure 1(a) for simulation in CST MWS.

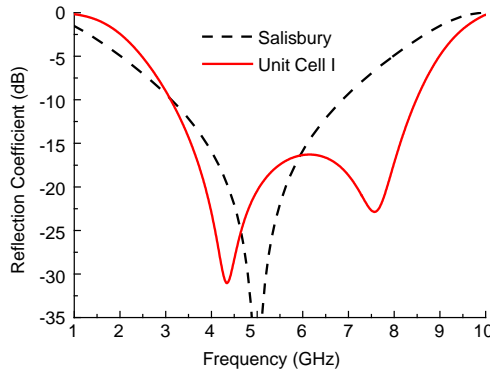


**Figure 3.** Predicted frequency response of Unit Cell I by using Floquet theory with the simulation result of conventional Salisbury screen absorber included for comparison, where resistance of the terminated load in Unit Cell I is  $150 \Omega$ .

absorber, which consists of Unit Cell I, is wider than that of the Salisbury screen absorber. The proposed absorber can reduce the thickness of the Salisbury screen by approximately 33%, demonstrating that a broadband antenna array can be applied to the design of a RAM. For the dual-polarization case in Unit Cell II against the incident angle, there is a slight variation in the absorption capability with small incident angle (Figure 4), where the vertical and horizontal polarization in this figure denotes that the incident electric field is along the  $y$  and  $x$  axes, respectively. There is a spurious dip (point A) at a angle of incidence  $\theta = 20^\circ$  in both polarization case, whose location shifts to a lower frequency as the angle of incidence increases. The dip can be ascribed to the existence of high order modes, and the cutoff frequency of the space harmonic ( $m, n$ ) is predictable as [23]

$$f_{c,mn} = \frac{C}{\cos^2\theta} \left\{ \begin{array}{l} \left( \frac{m}{a}p + \frac{n}{b}q \right) \\ + \sqrt{\left( \frac{m}{a}p + \frac{n}{b}q \right)^2 + \cos^2\theta \left[ \left( \frac{m}{a} \right)^2 + \left( \frac{n}{b} \right)^2 \right]} \end{array} \right\}, \quad (1)$$

$$p = \sin \theta \cos \phi$$

$$q = \sin \theta \sin \phi$$

where  $a$  and  $b$  are the periods along the  $x$ - and  $y$ -axes;  $\theta$  and  $\phi$  are the elevation and azimuth angles of the incident plane wave;  $C$  is the velocity of light in the free space. This figure shows that the proposed absorber composed of Unit Cell II possesses a wider bandwidth and dual-polarized operation mode.

Figure 5 shows the reflectance as a function of frequency at various

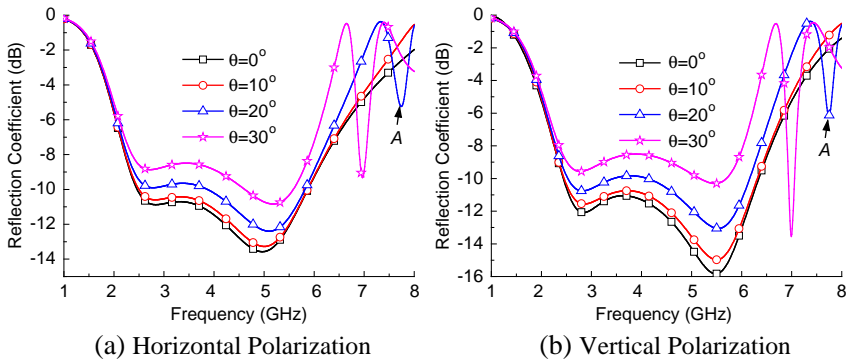


**Figure 4.** Frequency responses of Unit Cell II against the incident angle, where vertical and horizontal is denoted the different polarization of the incident wave. Both resistances of terminated loads are  $130 \Omega$ .

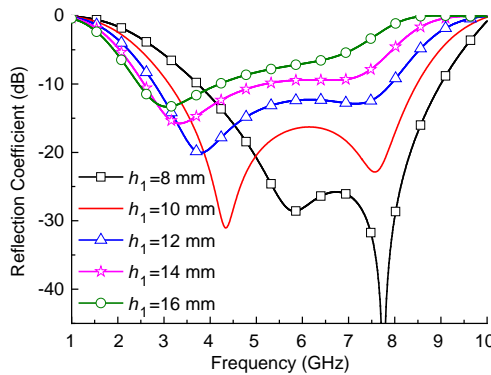


**Figure 5.** Reflectance as a function of frequency for thicknesses of the air foam,  $h_1$ , for Unit Cell I.

thicknesses of the air,  $h_1$ , for the single-polarization design. The dip location shifts to a lower frequency as the thickness increases, and the phenomenon of impedance mismatch becomes more obvious. According to the image theory, a dipole antenna oriented parallel to a perfect ground plane produces an image that carries the same magnitude current but is out of phase. This image dipole degrades the performance of the original dipole, which becomes more serious as the distance between the dipole antenna and the ground plane decreases. Therefore, a tradeoff must be made between the lowest operation frequency and the thickness.

#### 4. DESIGN EXAMPLES AND EXPERIMENTAL VERIFICATION

This section presents two types of absorbers for RCS reduction (Figure 6). Plastic threaded spacers were adopted to support the periodic bowtie structure printed on an FR-4 substrate at a constant distance above the ground plane. To minimize the influence of plastic spacers, their locations were considered in the simulation. Figure 6(a) shows that a  $540\text{ mm} \times 324\text{ mm}$  planar absorber has 18-by-12 unit cells composed of a bowtie in Unit Cell I. Figure 7 shows the simulated bi-static RCS of this absorber on the  $xz$ - and  $yz$ -planes at 5 GHz, where the excitation is a plane wave with vertical polarization propagating from the  $+z$  to the  $-z$  direction at a normal incidence. This figure also shows the bi-static RCS for the PEC plate of the same size

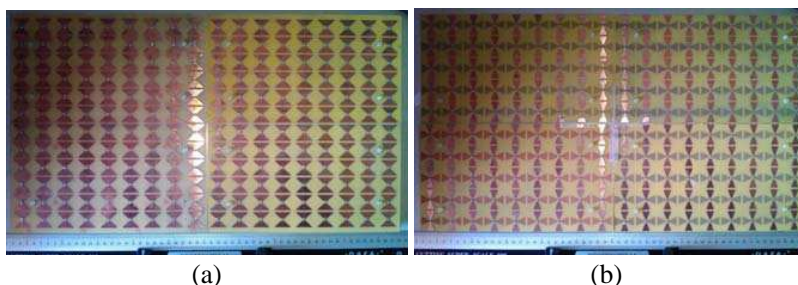


**Figure 6.** Photographs of the manufactured prototypes for (a) single- and (b) dual-polarization.

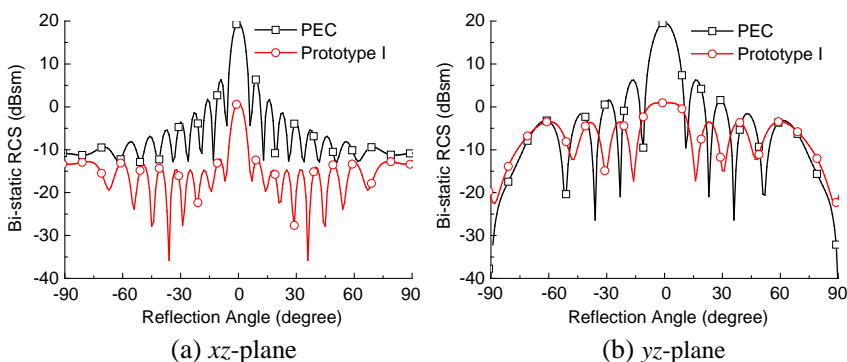


**Figure 7.** Simulated bi-static RCS of Prototype I in Figure 6 for vertical polarized incident wave on (a)  $xz$ - and (b)  $yz$ -plane at 5 GHz.

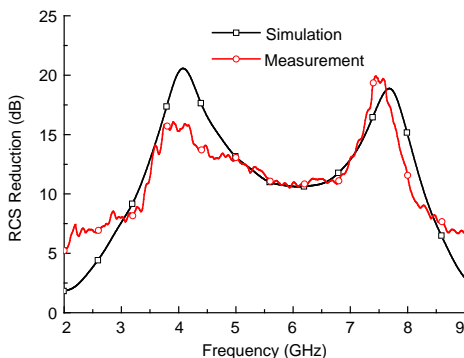


**Figure 8.** Simulated and measured RCS reductions at normal incident for Prototype I.

for comparison. The absorber dissipates the impinging wave rather than redirecting it away from the incident direction. Figure 8 shows the simulated and measured RCS reductions at a normal incidence, demonstrating excellent agreement between both results. The RCS reduction is the ratio of the mono-static RCS of the proposed absorber to that of the same size PEC plate. The operating band extends from 3.4 GHz up to 8.07 GHz for 10 dB RCS reduction, corresponding to an 81% bandwidth.

Figure 6(b) shows how the 18-by-10 unit cells composed of two cross bowties with the chip resistors in Unit Cell II form a 540 mm × 300 mm planar absorber. Figures 9 and 10 show the simulated bi-static

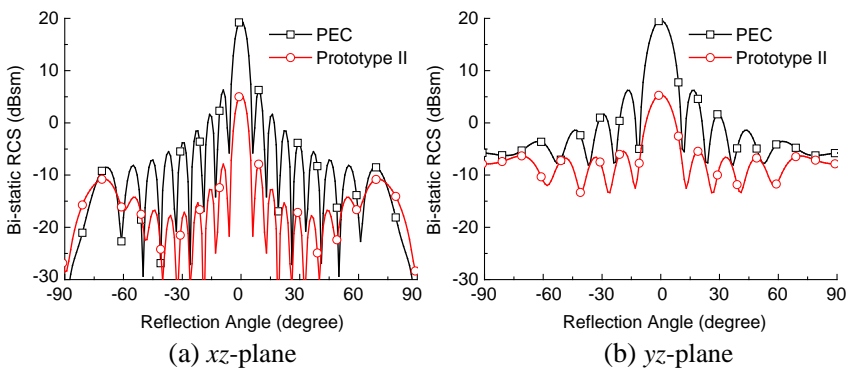


**Figure 9.** Simulated bi-static RCS of Prototype II in Figure 6(b) for horizontal polarized incident wave on (a)  $xz$ - and (b)  $yz$ -plane at 5 GHz.

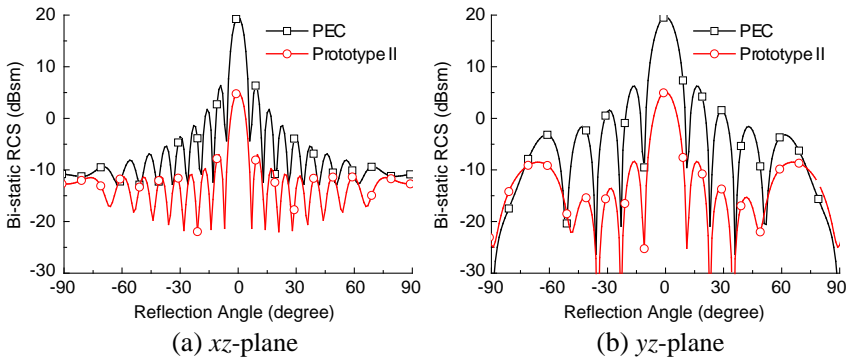


**Figure 10.** Simulated bi-static RCS of Prototype II in Figure 6(b) for vertical polarized incident wave on (a)  $xz$ - and (b)  $yz$ -plane at 5 GHz.

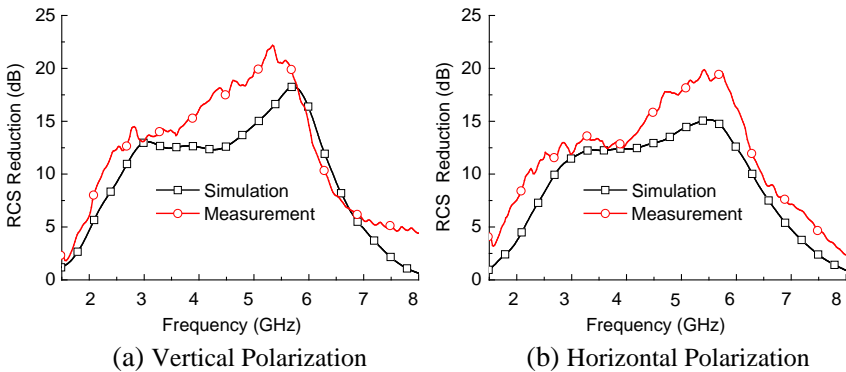


**Figure 11.** Simulated and measured RCS reduction at normal incident with (a) vertical- and (b) horizontal-polarization Prototype II in Figure 6(b).

RCS of this absorber on different cut planes at 5 GHz, and include a PEC plate of the same size for comparison. Figure 11 shows the simulated and measured RCS reduction at a normal incidence with various polarizations. At a 10 dB RCS reduction, the proposed dual-polarized absorber has 95% and 98% bandwidth at normal incidence with vertical and horizontal polarization, respectively.

To further demonstrate the performance of the proposed absorbers, we used a ground-penetrating radar for verification. The ultra-wideband radar system used in this study consisted of a pulse generator, a sampling converter, and a pair of antennas (Figure 12), and a personal computer was used to acquire the signal data. This

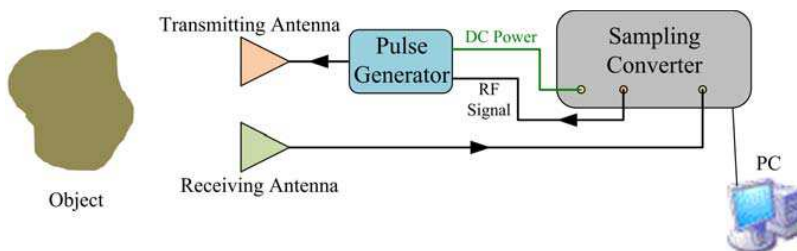


**Figure 12.** Ultra-wideband radar system consisted of a pulse generator, a sampling converter, and a pair of antennas.

radar system can measure the distance from the radar antenna to an object by calculating the time interval between signal transmission and reception. The spectrum of the pulse signal transmitted by the radar system ranges from 3 GHz to 6 GHz. Figure 13 shows the measured results for single- and dual-polarization designs, respectively, where the vertical axis is the signal amplitude and the horizontal axis is the distance expressed in meters. The device under test (DUT) was placed approximately 1.5 m away from the antennas of the radar system during measurement. In Figure 13 there is a pulse shaped signal at a distance of 1.5 m for the PEC case, confirming that this radar can accurately detect the distance from the radar antenna to an object. However, the proposed absorber can conceal the return signals of the radar system within the background noise.

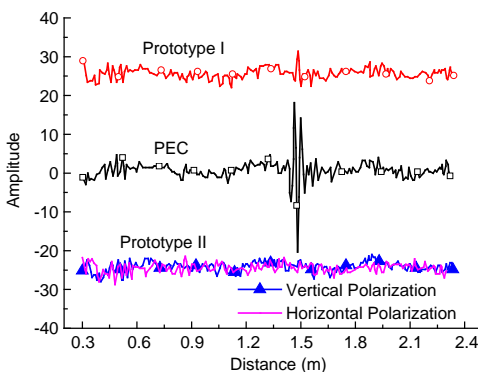


**Figure 13.** Reflected return signals of each DUT which is measured using a commercial ground-penetrating radar system. (The signals are upward and downward shifted by 25 units of amplitude for the cases of Prototype I and Prototype II.)

### 5. EQUIVALENT CIRCUIT MODEL

To speed up the analysis of the proposed absorber, a modified equivalent circuit model based on the RLC absorber [24] was developed to interpret the characteristics of the wideband absorption. Figure 14(a) shows the equivalent circuit model, in which a shunt RLC and two cascaded transmission lines connected in series are employed to model the absorbing structure. The capacitor  $C$  and inductor  $L$  are provided by the parasitic effects of the bowtie structure, and the resistor  $R$  represents the loss of the resistive load, metal, and so on. In addition, the substrate and air foam with conducting plate are modeled by cascading a short-circuited transmission line.

Figure 15 shows the imaginary parts of the admittances of the

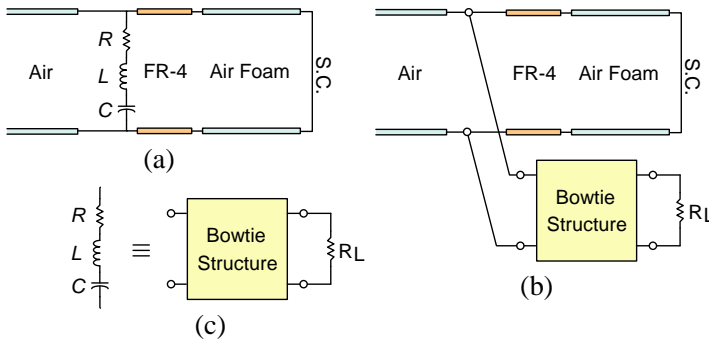


**Figure 14.** Equivalent circuit model for the wideband absorber.

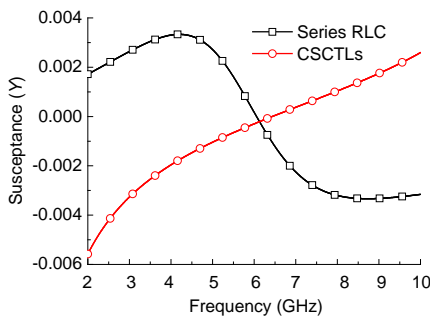


**Figure 15.** Imaginary parts of the admittances of the series RLC resonant ( $R = 150 \Omega$ ,  $C = 131 \text{ fF}$ , and  $L = 5.27 \text{ nH}$ ) and cascaded short-circuited transmission lines (CSCTLs).

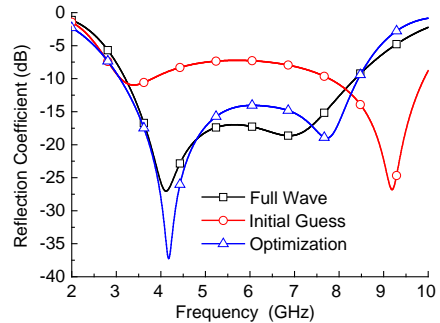


**Figure 16.** Reflection coefficient of equivalent circuit model with initial RLC values and optimized values ( $R = 292 \Omega$ ,  $C = 91.3 \text{ fF}$ , and  $L = 10 \text{ nH}$ ).

series RLC and cascaded short-circuited transmission lines. Here, the initial value of capacitor  $C$  can be determined by calculating the capacitance matrix of bowtie structure in electrostatics, and  $L$  is resonant with  $C$  at the center frequency of the absorber. The trends of the susceptances alternate inductively and capacitively with the frequency, implying that they may cancel each other. Figure 16 shows the result of the combination equivalent circuit in Figure 14(a) based on the initial guess values shown in Figure 15. An optimization procedure can be performed to find the parameters,  $R$ ,  $L$ , and  $C$ , so that the modeled frequency response can best fit with that of the absorber in the desired frequency band. The shunt RLC circuit was adopted to model the bowtie structure to ensure matching between the free space and the resistive load. In other words, the bowtie structure transforms the wave impedance into the lumped resistance  $R_L$  as shown in Figure 14(b). Therefore, the equivalent resistance  $R$  of the bowtie structure with resistive load is close to the free-space intrinsic impedance. The resistor  $R$  in the circuit model represents the real part of the impedance of the overall bowtie structure rather than a resistive load (Figure 14(c)).

## 6. CONCLUSION

This study presents a novel design of an ultra-thin absorber based on a wideband antenna array for the absorption of normal incident waves with single- or dual-polarization. Through analysis of unit cell of this wideband antenna array, the design of the absorber can be simplified. Two design examples were simulated, fabricated, and measured. Both designs have a bandwidth over 81% of 10 dB RCS reduction, and the thicknesses are less than 12% of the free space wavelength at the lowest operating frequency. Commercial ground-penetrating radar was used for performance verification, confirming the high RCS reduction of the proposed absorbers.

## ACKNOWLEDGMENT

We gratefully acknowledge the support of CST<sup>TM</sup> in providing software for numerical simulation.

## REFERENCES

1. Paquay, M., J. C. Iriarte, I. Ederra, R. Gonzalo, and P. de Maagt, "Thin AMC structure for radar cross-section reduction," *IEEE Transactions on Antennas and Propagation*, Vol. 55, No. 12, 3630–3638, 2007.

2. Zhang, Y., R. Mittra, and B. Wang, "Novel design for low-RCS screens using a combination of dual-AMC," *IEEE Antennas and Propagation Society International Symposium (APSURSI' 09)*, 1–4, 2009.
3. Zhang, Y., R. Mittra, B. Z. Wang, and N. T. Huang, "AMCs for ultra-thin and broadband RAM design," *Electronics Letters*, Vol. 45, No. 10, 484–485, 2009.
4. Tsai, Y. and R. Hwang, "RCS reduction of a composite AMC structure," *IEEE International Workshop on Electromagnetics, Applications and Student Innovation (iWEM 2011)*, 210–213, 2011.
5. Knott, E., J. Shaeffer, and M. Tuley, *Radar Cross Section*, SciTech Publishing, 2004.
6. Salisbury, W. W., "Absorbent body for electromagnetic waves," US Patent No. 2599944, 1952.
7. Landy, N., S. Sajuyigbe, J. Mock, D. Smith, and W. Padilla, "Perfect metamaterial absorber," *Physical Review Letters*, Vol. 100, No. 20, 207402, 2008.
8. Lee, J. and S. Lim, "Bandwidth-enhanced and polarisation-insensitive metamaterial absorber using double resonance," *Electronics Letters*, Vol. 47, No. 1, 8–9, 2011.
9. Wang, T., Z. Liao, H. Luo, and R. Gong, "Magnetic resonance coupling for extending perfect absorbance bandwidth at microwave frequencies," *IEEE International Conference on Ultra-Wideband (ICUWB 2010)*, Vol. 2, 1–4, 2010.
10. Abdalla, M. A., "Experimental verification of a triple band thin radar absorber metamaterial for oblique incidence applications," *Progress In Electromagnetics Research Letters*, Vol. 39, 63–72, 2013.
11. He, X.-J., Y. Wang, J. Wang, T. Gui, and Q. Wu, "Dual-band terahertz metamaterial absorber with polarization insensitivity and wide incident angle," *Progress In Electromagnetics Research*, Vol. 115, 381–397, 2011.
12. Fallahzadeh, S., K. Forooraghi, and Z. Atlasbaf, "Design, simulation and measurement of a dual linear polarization insensitive planar resonant metamaterial absorber," *Progress In Electromagnetics Research Letters*, Vol. 35, 135–144, 2012.
13. Zhu, B., Z. Wang, C. Huang, Y. Feng, J. Zhao, and T. Jiang, "Polarization insensitive metamaterial absorber with wide incident angle," *Progress In Electromagnetics Research*, Vol. 101, 231–239, 2010.

14. Li, M., H. Yang, X. Hou, Y. Tian, and D. Hou, "Perfect metamaterial absorber with dual bands," *Progress In Electromagnetics Research*, Vol. 108, 37–49, 2010.
15. Huang, L. and H. Chen, "Multi-band and polarization insensitive metamaterial absorber," *Progress In Electromagnetics Research*, Vol. 113, 103–110, 2011.
16. Seman, F., R. Cahill, and V. Fusco, "Performance enhancement of salisbury screen absorber using a resistively loaded high impedance ground plane," *Proceedings of the Fourth European Conference on Antennas and Propagation (EuCAP 2010)*, 1–5, 2010.
17. Seman, F. and R. Cahill, "Performance enhancement of salisbury screen absorber using resistively loaded spiral FSS," *Microwave and Optical Technology Letters*, Vol. 53, No. 7, 1538–1541, 2011.
18. Seman, F., R. Cahill, V. Fusco, and G. Goussetis, "Design of a salisbury screen absorber using frequency selective surfaces to improve bandwidth and angular stability performance," *IET Microwaves, Antennas & Propagation*, Vol. 5, No. 2, 149–156, 2011.
19. Costa, F., A. Monorchio, and G. Manara, "Analysis and design of ultra thin electromagnetic absorbers comprising resistively loaded high impedance surfaces," *IEEE Transactions on Antennas and Propagation*, Vol. 58, No. 5, 1551–1558, 2010.
20. Pang, Y.-Q., Y.-J. Zhou, and J. Wang, "Equivalent circuit method analysis of the influence of frequency selective surface resistance on the frequency response of metamaterial absorbers," *Journal of Applied Physics*, Vol. 110, No. 2, 023704-1–023704-5, 2011.
21. Lee, W., J. Lee, and C. Kim, "Characteristics of an electromagnetic wave absorbing composite structure with a conducting polymer electromagnetic bandgap (EBG) in the X-band," *Composites Science and Technology*, Vol. 68, No. 12, 2485–2489, 2008.
22. "CST studio suite 2012," <http://www.cst.com>.
23. Hwang, R.-B., *Periodic Structures: Mode-matching Approach and Applications in Electromagnetic Engineering*, Wiley-IEEE Press Publishing, 2012.
24. Rashid, A., Z. Shen, and R. Mittra, "On the optimum design of a single-layer thin wideband radar absorber," *IEEE International Symposium on Antennas and Propagation (APSURSI 2011)*, 2916–2919, 2011.